Макрогетероциклы
http://macroheterocycles.isuct.ru

DOI: 10.6060/mhc201026z

Complexes of Ca(II), Ni(II) and Zn(II) with Hemi– and Dicarbahemiporphyrazines: Molecular Structure and Features of Metal–Ligand Bonding

Alexey V. Eroshin, Arseniy A. Otlyotov, Yuriy A. Zhabanov,[@]
Vladimir V. Veretennikov, and Mikhail K. Islyaikin

Ivanovo State University of Chemistry and Technology, Research Institute of Chemistry of Macroheterocyclic Compounds, 153000 Ivanovo, Russian Federation
[@]Corresponding author E-mail: zhabanov@isuct.ru

Equilibrium geometry and electronic structures of Ca(II), Ni(II) and Zn(II) complexes with hemi- and dicarbahemiporphyrazines were determined by DFT calculations at PBE0/pcseg-2 level followed by natural bond orbital (NBO) analysis of the electron density distribution. Electronic structures of Ni(II) complexes in ground and low-lying excited electronic states were determined by complete active space (CASSCF) method with following accounting dynamic correlation by multiconfigurational quasidegenerate second-order perturbation theory (MCQDPT2). According to data obtained by MCQDPT2 method the complexes of hemi- and dicarbahemiporphyrazine possess the ground states $^1A_1$ and $^3B_1$, respectively, and wave functions of the ground states have the form of a single determinant in the case of Ni(II) complex with hemiporphyrazine and the wave function for Ni(II) with dicarbahemiporphyrazine were found to possess a complex composition, therefore this complex could not be treated using single-reference DFT methods. The covalent component of metal-ligand bonding was found to increase significantly in the series: Ca(II) → Zn(II) → Ni(II). Large covalent contribution into Ni–N bonding is explained by additional LP(Np) → $3d_{x^2-y^2}$(Ni) and LP(Ni) → $3d_{x^2-y^2}$(Ni) interactions. The presence of agostic interactions -C–H···Zn in the dicarbahemiporphyrazine complex was also confirmed.

Keywords: Hemiporphyrazines, natural bond orbital analysis, DFT, chemical bonding, aromaticity, nucleus-independent chemical shift.

Комплексы геми– и дикарбагемипорфиразинов с Ca(II), Ni(II) и Zn(II): молекулярная структура и особенности химической связи металл–лиганд

А. В. Ерошин, А. А. Отлетов, Ю. А. Жабанов,[@] В. В. Веретенников,
М. К. Исляйкин

Ивановский государственный химико-технологический университет, Научно-исследовательский институт химии макрогетероциклических соединений, 153000 Иваново, Россия
[@]E-mail: zhabanov@isuct.ru

Геометрическое и электронное строение комплексов геми- и дикарбагемипорфиразина с Ca(II), Ni(II) и Zn(II) были определены методом DFT на уровне PBE0/pcseg-2 с последующим анализом распределения электронной плотности по методу NBO. Электронная структура комплексов Ni(II) в основном и низколежащих возбужденных электронных состояниях была определена с помощью метода самосогласованного поля в полном активном пространстве (CASSCF) с последующим учетом динамической корреляции по многофункциональной квазивырожденной теории возмущений второго порядка (MCQDPT2). Согласно данным, полученным по методу MCQDPT2, комплексы геми- и дикарбагемипорфиразина обладают основными состояниями $^1A_1$ и $^3B_1$, соответственно. Волновые функции основного состояния в случае гемипорфиразина Ni(II) являются однодетерминантными, а в случае дикарбагемипорфиразина Ni(II) оказались многодетерминантными,

поэтому этот комплекс не может быть изучен при помощи однодетрминантных методов теории функционала плотности. Было обнаружено, что ковалентная составляющая связи металл-лиганд существенно возрастает в ряду Ca(II) → Zn(II) → Ni(II). Высокий ковалентный вклад в связь Ni-N может быть объяснен дополнительными взаимодействиями LP(N_p) → 3$d_{x^2-y^2}$(Ni) и LP(N_i) → 3$d_{x^2-y^2}$(Ni). Также было подтверждено наличие агостических взаимодействий C–H···Zn в комплексе дикарбагемипорфиразина.

Ключевые слова: Гемипорфиразин, NBO-анализ, DFT, химическая связь, ароматичность, ядерно-независимый химический сдвиг.

Introduction

Macroheterocycles, such as porphyrins, phthalocyanines, their analogues and metal complexes form the large class of compounds with a broad range of applications. Hemiporphyrazine (H_2hp) and dicarbahemiporphyrazine (H_2dchp) and their metal complexes have been attracting scientific and practical interest,[1–6] such as optical limiters,[7,8] excitonic luminescence,[9] nonlinear optical and photoelectronic materials.[10–12] A number of works are devoted to the study of the structure of this class of compounds.[13–17]

One of the fundamental problems of macroheterocycles is the aromaticity of the macrocyclic system. Phthalocyanines are characterized by an aromatic macroring bearing 18 π-electrons which causes them to absorb light from the red region of the spectrum assuming their blue color. H_2hp and H_2dchp molecules can be considered as structural analogues of Pc in the molecule of which two opposite faced isoindole subunits are replaced by rests of aromatic diamines. As a consequence, it interrupts the conjugation around the macrocycle and shifts light absorption into 300–450 nm region, thereof an enhancement of color from blue to yellow-orange takes place. Recently it was shown that in the case of H_2dchp perturbation of local aromaticity of 1,3-phehylene rings by transformation it in quinoidal form by introducing of carbonyl groups in 4- or/and 6-positions induces appearance of global aromaticity, *i.e.* aromaticity of inner macroring.[18,19] The maximum of absorption was found to be located at *ca.* 800 nm.

Since the structure and properties of the metal complexes of macroheterocycles are predominantly determined by the size of coordination cavity of a macrocycle and ionic radius of a metal, accurate structural data are necessary to reveal structure-properties relationship and trends in the properties of these compounds. Recently, a considerable literature has grown up around the metal chemistry of hemi- and carbahemiporphyrazines (the detailed review can be found in Ref. [4]). The present contribution aims to extend our recent studies of the structure of metal complexes[20,21] by considering complexes of Ca(II), Ni(II) and Zn(II) with different ligands – hemiporphyrazine (**hp**) and dicarbahemiporphyrazine (**dchp**). For comparative studies of the influence of transition metal and ligand on the chemical bonding and spectral properties it is reasonable to consider the relatively simple borderline closed-shell d^0 and d^{10} configurations (Ca and Zn, respectively). The choice of complexes with nickel as objects of study is due to the rather high interest in these complexes according to the literature.[22–28] The solid-state structures obtained by X-ray structural analysis are reported for **Mhp** and **Mdchp** complexes (**M** = Ni, Zn). The complex **Nihp** possesses a saddle distorted structure of macrocycle,[23] while in the case of a structure with two pyridine moieties as axial ligands the macrocycle exhibits ruffling distortion.[27] The structure of externally protonated **Nidchp** is a square planar with a slightly warped out of plane macrocycle.[26] The macrocyclic ligand of **Znhp** is almost planar,[24,29] while the Zn(II) adduct of dicarbahemiporphyrazine has a saddle distorted macrocycle.[30] The gas-phase structures and thermal properties of free base hemiporphyrazine (**H_2hp**) and dicarbahemiporphyrazine (**H_2dchp**) have been recently determined in our laboratory by gas-phase electron diffraction[31] and Knudsen effusion method with mass spectrometric control of vapor composition.[32] However, there has been no detailed investigation of the structures and properties of free **Mhp** and **Mdchp** (**M** = Ca, Ni, Zn) molecules (Scheme 1) in the gas phase, where molecular structures are not distorted by collective interactions. The objectives of this research are to determine the equilibrium structures and by quantum-chemical calculations and to describe the features of metal binding in the framework of NBO analysis of electron density distribution. Besides, the influence of molecular structure on electronic absorption spectra is discussed.

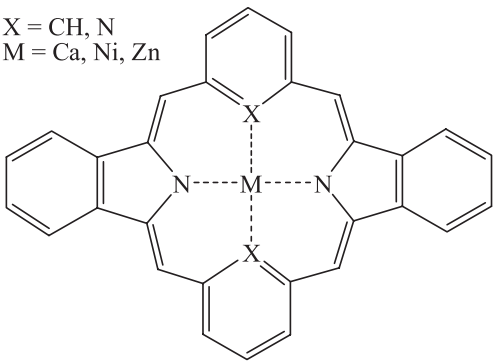

Scheme 1. Molecular model of **Mhp** (X = N) and **Mdchp** (M = CH) complexes.

Computational Details

The electronic configurations of Ca(II) and Zn(II) are relatively simple borderline [Ar]d^0 and [Ar]d^{10}. Consequently the closed-shell Mhp and Mdchp complexes with Ca and Zn can be treated using single-reference DFT method. The electronic configuration of Ni(II) is [Ar]$3d^8$, therefore, it can form in ground

state either singlet, or triplet complexes. Furthermore, the computational investigations in the case of Ni(II) complexes are often non-trivial due to the necessity to account for the multireference character of the wavefunction.

The electronic structures of **Nihp** and **Nidchp** have been studied by CASSCF method followed by accounting for dynamic electron correlation by multiconfigurational quasidegenerate second-order perturbation theory (MCQDPT2). Eight electrons in five molecular orbitals consisting mainly of the 3d orbitals of Ni atom were selected for the active space. The doubly occupied orbitals corresponding to 1s orbitals of C, N, Ni and the 2s and 2p orbitals of Ni were frozen in the MCQDPT2 calculations. The triple-zeta basis sets pcseg-2[33] from the Basis Set Exchange database[34,35] were used in all calculations. The wave functions for singlet and triplet states of **Nidchp** were found to possess a complex composition (Table 1), therefore **Nidchp** could not be treated using single-reference DFT methods.

DFT/PBE0-based investigations of **Mhp** (**M** = Ca, Ni, Zn) and **Mdchp** (**M** = Ca, Zn) included geometry optimizations followed by computations of harmonic vibrations and TDDFT calculations of the electronic absorption spectra. The number of the calculated excited states was 30. All calculations were performed using the Firefly QC package,[36] which is partially based on the GAMESS (US)[37] source code.

The molecular models and orbitals demonstrated in the paper were visualized by means of the Chemcraft program.[38]

Results and Discussion

*Electronic states of **Nihp** and **Nidchp***

The compositions of the wave functions are presented in Table 1 for the low-lying electronic states. According to the data obtained by MCQDPT2 method **Nihp** and **Nidchp** complexes possess the ground states $^1A_1$ and $^3B_1$, respectively. The low-lying triplet and singlet states of **Nihp** and **Nidchp** compounds are by 89.9 and 180.0 kJ·mol^{-1} higher in energy than the corresponding ground states (Table 1). It should be noted that, according to CASSCF calculations, **Nihp** possesses a triplet ground state. Such contradictory conclusions about the multiplicity of the ground state obtained using the CASSCF and MCQDPT2 methods are apparently due to the fact that the CASSCF calculations with a small active space do practically not take into account the dynamic correlation of electrons.

Analysis of the data in Table 1 demonstrates that the wave functions of the ground state and the most low-lying singlet states of **Nihp** have the form of a single determinant.

Shapes of CASSCF active molecular orbitals (Figure 1) and their composition analysis show that the corresponding components of the d-orbitals of the metal atom make a dominant contribution to them in cases of triplet state of **Nihp** and all states of **Nidchp**. The orbitals of the macrocycle atoms are almost not involved in the formation of these molecular orbitals. The orbital of $41a_1$ symmetry is an exception, since according to Figure 1 the contribution of the macrocycle orbitals can be visually observed. It should be noted that no noticeable interaction of metal d-orbitals and macrocycle orbitals was found for triplet state of **Nihp** and triplet state of **Nidchp**. Thus, the crystal field theory (CFT) can be used to describe the sequence of electronic states given in Table 1 in all cases, except for singlet state of **Nihp**. In the framework of the theory of the crystal field, the most energetically favorable states are those with the least repulsion between the electrons occupying the d-shell of the metal and orbitals of the macrocycle. From this point of view, the occupation of the $24a_2$, $31b_2$, $40a_1$, and $32b_1$ MOs are the most favorable, but not $41a_1$. Similar conclusions were made by the authors for iron and cobalt complexes of porphyrazine and tetra(1,2,5-thiadiazole)porphyrazine.[21] It should be noted that no noticeable interaction of metal d-orbitals and orbitals of carbon atoms in benzene

Table 1. The relative energies (kJ·mol^{-1}) of excited states and contributions (in %) of electronic configurations to the wave functions from MCQDPT2 calculations.

State	Contributions	ΔE, kJ·mol^{-1}
	Nihp	
$^1A_1$	$100[(31b_1)^2(24a_2)^2(32b_1)^2(40a_1)^2(41a_1)^0]$	0.0
$^1B_1$	$99[(31b_1)^2(24a_2)^2(32b_1)^1(40a_1)^2(41a_1)^1]$	309.6
$^1A_2$	$100[(31b_1)^2(24a_2)^1(32b_1)^2(40a_1)^2(41a_1)^1]$	438.8
$^1A_1$	$97[(31b_1)^2(24a_2)^2(32b_1)^2(40a_1)^1(41a_1)^1]$	445.0
$^1B_1$	$99[(31b_1)^1(24a_2)^2(32b_1)^2(40a_1)^2(41a_1)^1]$	516.4
$^3B_1$	$15[(24a_2)^2(40a_1)^1(31b_2)^2(32b_1)^1(41a_1)^2]+$ $84[(24a_2)^2(40a_1)^2(31b_2)^2(32b_1)^1(41a_1)^1]$	89.9
$^3A_1$	$100[(24a_2)^2(40a_1)^1(31b_2)^2(32b_1)^2(41a_1)^1]$	104.5
$^3B_2$	$98[(24a_2)^2(40a_1)^2(31b_2)^1(32b_1)^2(41a_1)^1]$	115.5
$^3A_2$	$30[(24a_2)^2(40a_1)^2(31b_2)^1(32b_1)^1(41a_1)^2]+$ $69[(24a_2)^1(40a_1)^2(31b_2)^2(32b_1)^2(41a_1)^1]$	194.9
$^3B_2$	$18[(24a_2)^2(40a_1)^1(31b_2)^1(32b_1)^2(41a_1)^2]+$ $81[(24a_2)^1(40a_1)^2(31b_2)^2(32b_1)^1(41a_1)^2]$	343.0
	Nidchp	
$^1A_1$	$87[(31b_2)^2(40a_1)^2(32b_1)^2(24a_2)^2(41a_1)^0]+$ $6[(31b_2)^2(40a_1)^1(32b_1)^2(24a_2)^2(41a_1)^1]$	180.0
$^1B_1$	$96[(31b_2)^2(40a_1)^2(32b_1)^1(24a_2)^2(41a_1)^1]$	370.9
$^1B_2$	$86[(31b_2)^1(40a_1)^2(32b_1)^2(24a_2)^2(41a_1)^1]+$ $8[(31b_2)^2(40a_1)^2(32b_1)^1(24a_2)^1(41a_1)^2]+$ $6[(31b_2)^1(40a_1)^1(32b_1)^2(24a_2)^2(41a_1)^2]$	403.0
$^1A_1$	$84[(31b_2)^2(40a_1)^1(32b_1)^2(24a_2)^2(41a_1)^1]+$ $6[(31b_2)^2(40a_1)^2(32b_1)^0(24a_2)^2(41a_1)^2]$	410.6
$^1A_2$	$92[(31b_2)^2(40a_1)^2(32b_1)^2(24a_2)^1(41a_1)^1]+$ $7[(31b_2)^2(40a_1)^1(32b_1)^2(24a_2)^1(41a_1)^2]$	453.4
$^3B_1$	$30[(31b_1)^1(40a_1)^2(24a_2)^2(32b_1)^2(41a_1)^1]+$ $67[(31b_1)^2(40a_1)^2(24a_2)^2(32b_1)^1(41a_1)^1]$	0.0
$^3A_1$	$100[(31b_1)^2(40a_1)^1(24a_2)^2(32b_1)^2(41a_1)^1]$	64.6
$^3B_2$	$29[(31b_1)^1(40a_1)^2(24a_2)^1(32b_1)^2(41a_1)^2]+$ $71[(31b_1)^2(40a_1)^2(24a_2)^1(32b_1)^1(41a_1)^2]$	121.6
$^3B_1$	$68[(31b_1)^1(40a_1)^2(24a_2)^2(32b_1)^2(41a_1)^1]+$ $29[(31b_1)^2(40a_1)^2(24a_2)^2(32b_1)^1(41a_1)^1]$	129.7
$^3A_2$	$87[(31b_1)^2(40a_1)^1(24a_2)^1(32b_1)^2(41a_1)^2]+$ $13[(31b_1)^2(40a_1)^2(24a_2)^1(32b_1)^2(41a_1)^1]$	146.5

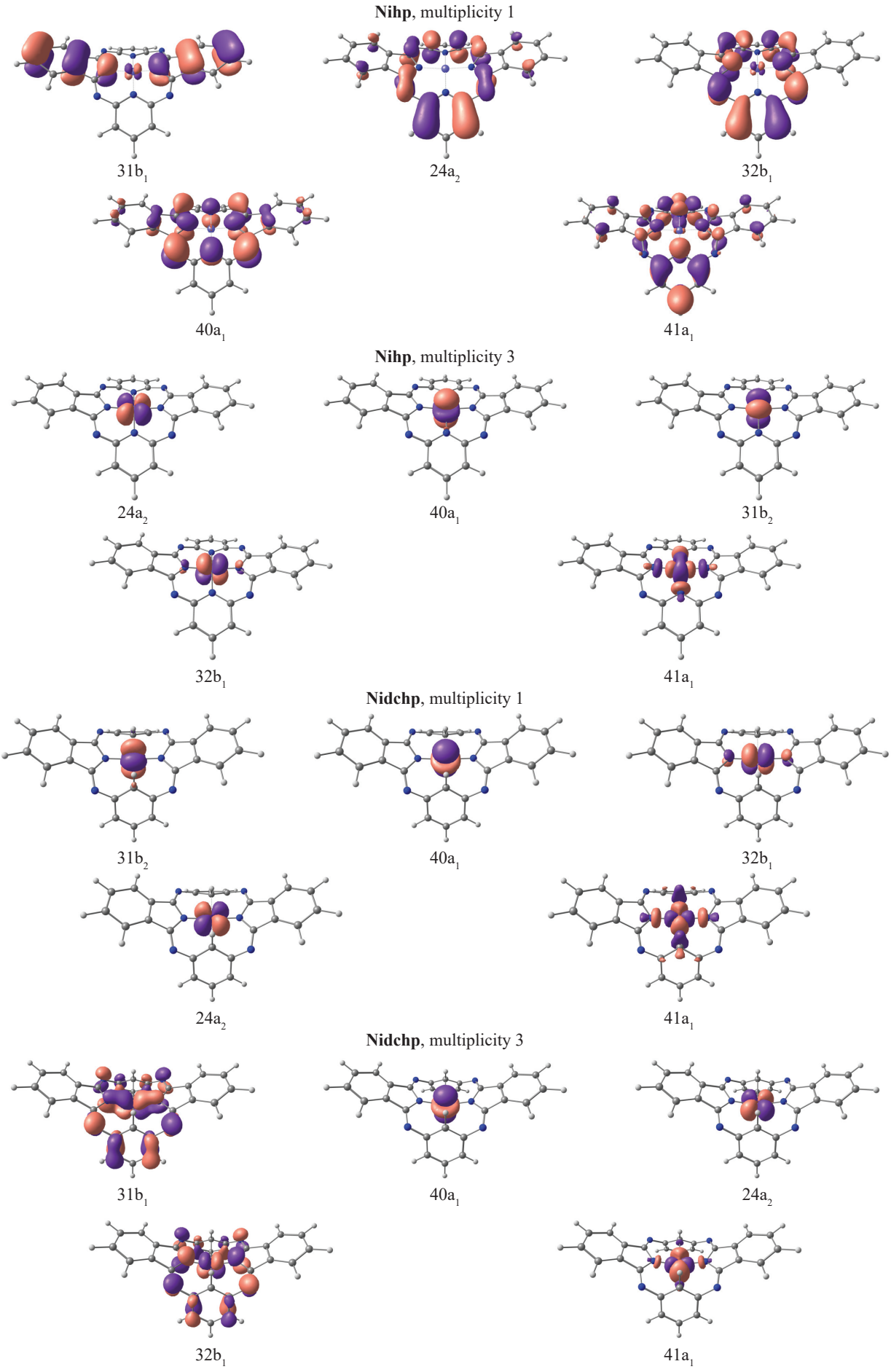

Figure 1. Shapes of active CASSCF molecular orbital structures and chemical bonding in **Mhp** and **Mdchp**.

moieties was found in **Nidchp** (Figure 1). Thus, the nickel atom is coordinated only by two nitrogen atoms of the pyrrole fragment, similar to a linear molecule. This can explain the stabilization of the triplet state, which is consistent with CFT. The electronic structure of NiX_2 (X = F, Cl, Br, I) molecules was determined in a similar approximation, and it was found that the ground state is a triplet.[39] It should be noted that the relative energies of the low-lying singlet states of NiX_2 molecules are in the range 152–158 kJ·mol^{-1},[39] which is compatible with the relative energy of the low-lying singlet states of **Nidchp** (180 kJ·mol^{-1}).

Shapes of CASSCF active molecular orbitals of singlet **Nihp** state comprise atoms of the macrocycle to a greater extent than the metal atom (Figure 1). Thus, for this case it is impossible to describe sequence of electronic states using the theory of the crystal field (CFT), and the consideration of a molecule as a system consisting of a cation of metal Ni^{2+} and a ligand anion $\mathbf{hp}^{2-}$ is not applicable.

According to our DFT computations, the complexes **Mhp** and **Mdchp** possess equilibrium structures of C_{2v} symmetry with saddle type distorted macrocyclic skeleton (Figure 2). Force-field calculations yielded no imaginary frequencies, indicating that the optimized configurations correspond to the minima on the potential energy hypersurfaces. Since complex compounds are usually represented as consisting of a positively charged central ion and a negatively charged ligand, in order to compare geometrical and electronic characteristics of the complexes and to study the influence of the nature of the metal on the structure of the macrocyclic skeleton we have determined the equilibrium structures of $\mathbf{[hp]}^{2-}$ and $\mathbf{[dchp]}^{2-}$ ions in the same approximation (PBE0/pcseg-2), which were determined to possess D_{2h} and C_{2v} symmetries, respectively. The calculated molecular parameters are presented in Table 2. Comparison of the geometric parameters of the studied complexes reveals that the the distances between the metal and nitrogen atoms of the pyrrole rings r(M-N) are changed in the sequence **Cadchp > Cahp > Zndchp > Znhp > Nihp**. It should be noted that this distance is similar with corresponding distance of porphyrazine and tetrakis(1,2,5-thiadiazole) porphyrazine complexes with Ca and Zn.[20] The nature of a metal atom significantly affects the shape of a macrocyclic ligand. Ca(II) induces the most pronounced distortion of **hp** and **dchp** ligands that is quantitatively expressed by the values of α(pyr/benz) angles (Figure 3, Table 2). In the case of **Cadchp**, the planes of the benzene moieties are almost parallel, α(pyr/benz) = 4.3°.

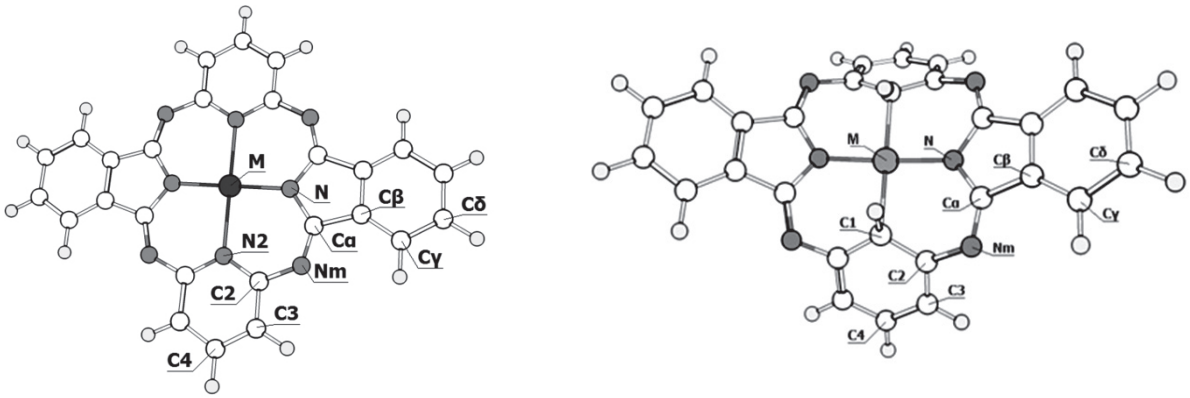

Figure 2. Molecular models of **Mhp** (right) and **Mdchp** (left) with atom labeling.

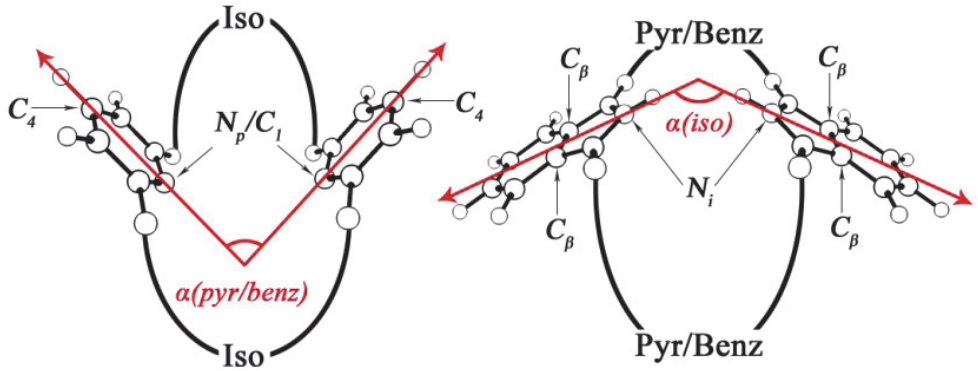

Figure 3. The definition of the dihedral angles that describe *saddle* distortion: α(pyr) = angle between vectors $\overrightarrow{N_pC_4}$ of the opposite faced pyridine fragments; α(benz) = angle between vectors $\overrightarrow{C_lC_4}$; α(iso) = angle between vectors $\overrightarrow{N_lX}$, where X is a dummy atom placed in the middle of C_β–C_β bonds.

Table 2. Molecular parameters (bond lengths in Å and bond angles in degrees) of **Mhp** and **Mdchp** (**M =** Ca, Ni, Zn) complexes and **[hp]$^{2-}$** and **[dchp]$^{2-}$** anionic forms optimized at PBE0/pcseg-2 level.

	[hp]$^{2-}$	**[dchp]$^{2-}$**	**Cahp**	**Nihp**	**Znhp**	**Cadchp**	**Zndchp**
M - N_2/C_1	–	–	2.400	2.014	2.225	2.790	2.396
M - N	–	–	2.229	1.873	1.919	2.357	1.937
C_2-N_m	1.385	1.386	1.381	1.361	1.370	1.389	1.383
C_α-N_m	1.297	1.299	1.288	1.279	1.282	1.286	1.279
N_p/C_1 - C_2	1.333	1.406	1.355	1.367	1.356	1.400	1.403
C_2-C_3	1.405	1.407	1.397	1.397	1.399	1.405	1.394
C_3-C_4	1.383	1.384	1.380	1.367	1.377	1.391	1.386
N_i-Cα	1.349	1.358	1.370	1.374	1.377	1.375	1.392
Cα-C_β	1.493	1.488	1.479	1.468	1.471	1.476	1.471
C_β-C_γ	1.381	1.383	1.382	1.382	1.382	1.381	1.383
C_γ-C_δ	1.394	1.392	1.390	1.390	1.389	1.390	1.388
$(N\ldots N)_i$	3.945	3.963	4.008	3.735	3.838	4.147	3.827
X-M	–	–	0.831	0.190	0.036	–1.288	–0.311
α(iso)	114.1	180	145.5	140.5	168.9	120.2	136.0
α(pyr/benz)	79.0	180	113.7	127.2	164.4	4.3	57.5

The comparison of the calculated structural parameters with the available X-ray data demonstrates significant (by ~ 0.09 Å in **Nihp**,[26] by ~ 0.04 Å in **Znhp** and by ~ 0.06 Å in **Zndchp**[30]) elongation of M–N distances in the solid state. The elongation is even larger in the case of Ni–N_2 (~ 0.17 Å[26]) and Zn–C (~ 0.08 Å[30]) bonds of **Nihp** and **Zndchp**, respectively.

The position of a metal atom relative to the macrocyclic fragment described by M–X distance (where X is a dummy atom located between the opposite N_p/C_1 atoms) also varies significantly in the series Ca(II) – Ni(II) – Zn(II). While Ni(II) and Zn(II) atoms are comparatively close to the in-plane positions, Ca(II) atoms exhibit large out-of-plane shift. Note, that the sign of the shift is different for **hp** and **dchp** complexes.

The structural features of **Mhp** and **Mdchp** complexes can be connected with the electron density distribution rationalized within the framework of the NBO method.[40] According to the values of the natural charges q(M) and Wiberg bond indices Q(M–N_p) and Q(M–N_{iso}), the complexes with Ca(II) can be considered as ionic species, while the complexes with Zn(II) and especially Ni(II) possess large covalent contributions into metal–ligand bonding (Table 3). The different nature of the chemical bonding can be also explained by comparison of the energies of donor-acceptor interactions between natural bond orbitals

Table 3. Selected parameters of **Mhp** and **Mdchp** (**M** = Ca, Ni, Zn) complexes from NBO analysis.

	Cahp	**Nihp**	**Znhp**	**Cadchp**	**Zndchp**
Δ*E*(HOMO-LUMO), eV	3.47	3.06	3.05	4.65	4.25
q(M) NPA, *e*	1.781	0.629	1.268	1.739	1.289
q(N_p) NPA, *e*	–0.630	–0.452	–0.555	–0.327	–0.424
q(N_i) NPA, *e*	–0.772	–0.547	–0.725	–0.796	–0.770
Configuration	$4s^{0.10}3d^{0.10}$	$4s^{0.29}3d^{8.68}4p^{0.40}4d^{0.01}$	$4s^{0.36}3d^{9.96}4p^{0.40}$	$4s^{0.10}3d^{0.10}$	$4s^{0.38}3d^{9.96}4p^{0.36}$
∑ *E*, kcal/mol	92	822	463	81	421
∑ *E* (M + benz/pyr), kcal/mol	39	292	152	34	97
∑ *E* (M + 2 iso), kcal/mol	50	526	307	40	318
Q(M-N_p), *e*	0.084	0.484	0.230	0.023	0.130
Q(M-N_i), *e*	0.109	0.545	0.376	0.111	0.405
r(M-N_p), Å	2.400	2.014	2.225	2.790	2.396
r(M-N_i), Å	2.229	1.873	1.919	2.357	1.937

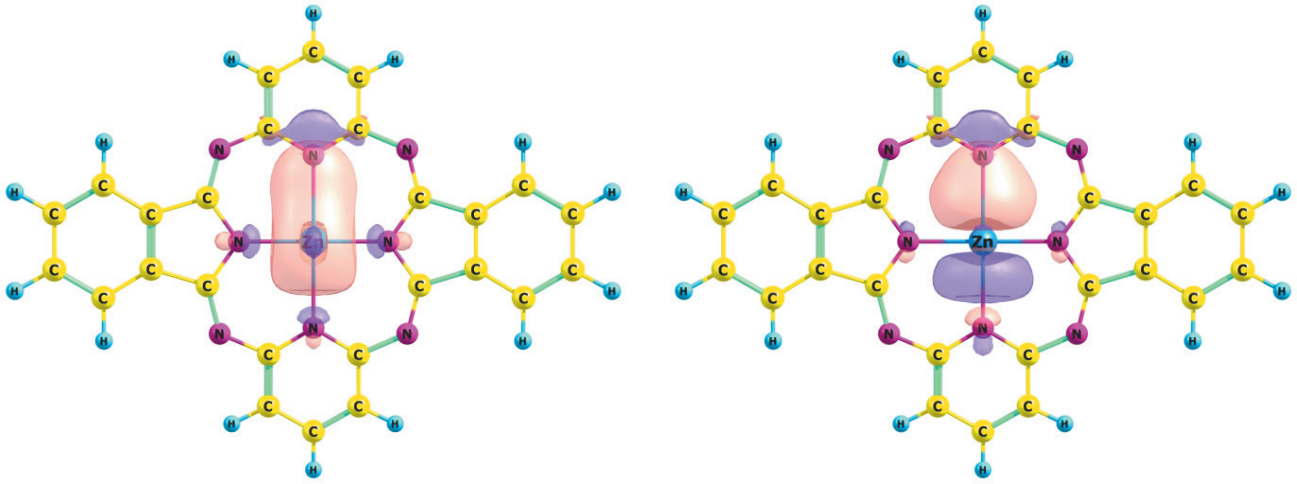

Figure 4. Schemes of the dominant donor-acceptor interactions between Zn and **hp** ligand. (a) The result of the orbital interaction of the type LP(N) → 4*s*(Zn) ($E^{(2)}$ = 28.9 kcal·mol^{-1}); (b) The result of the orbital interaction of the type LP(N) → 4*p*(Zn) ($E^{(2)}$ = 36.6 kcal·mol^{-1}). Only one of the two corresponding interactions is demonstrated.

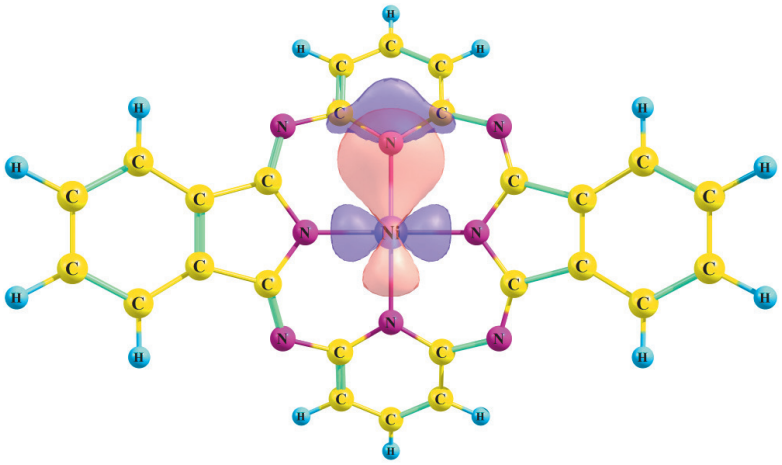

Figure 5. Scheme of the donor-acceptor interaction of the type LP(N) → $3d_{x^2-y^2}$(Ni) ($E^{(2)}$ = 35.6 kcal·mol^{-1}).

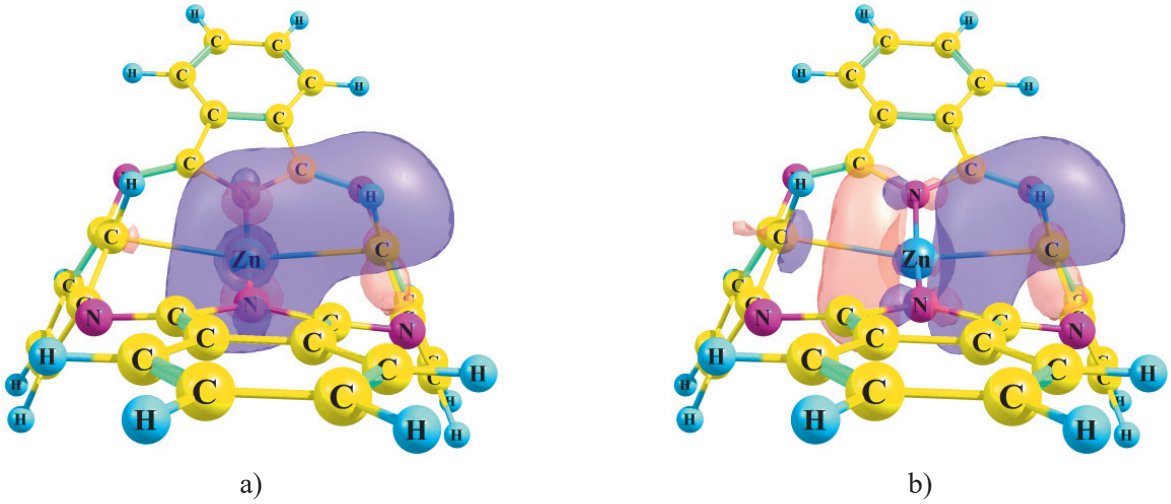

Figure 6. Schemes of the agostic donor-acceptor interactions in **Zndchp**: (a) The result of the orbital interaction of the type σ(C–H) → 4*s*(Zn) ($E^{(2)}$ = 5.1 kcal·mol^{-1}); (b) The result of the orbital interaction of the type σ(C–H) → 4*p*(Zn) ($E^{(2)}$ = 4.9 kcal·mol^{-1}).

of a metal atom acting as acceptors of the electron density and the donor orbitals of the macrocyclic fragment. The total energy ($\sum E$) can be decomposed into two main contributions: the energy of the interactions between metal atom and pyridine (**hp** complexes) or benzene (**dchp** complexes) moieties, denoted as $\sum E$ (M + 2 benz/pyr) and the energy of the interactions between central atom and isoindole fragments ($\sum E$ (M + 2 iso)). Each of these three energy quantities increases in the series Ca(II) → Zn(II) → Ni(II) for both **hp** and **dchp** complexes.

Znhp is stabilized by LP(N_p) → 4s(Zn), LP(N_p) → 4p(Zn), LP(N_i) → 4s(Zn) and LP(N_i) → 4p(Zn) interactions (Figure 4), while in the case of **Nihp** additional strong LP(N_p) → $3d_{x^2-y^2}$(Ni) and LP(N_i) → $3d_{x^2-y^2}$(Ni) interactions occur (Figure 5). Only much weaker orbital overlaps of the types LP(N_p) → 4s(Ca) and LP(N_i) → 4s(Ca) can be found in **Cahp** complex.

Analogues qualitative picture can be drawn for the **dchp** complexes. Besides, **Zndchp** complex is additionally stabilized by agostic interactions[41–43] (Figure 6)

Table 4. NICS(0) values (in ppm) at the center of the cyclic fragments of **Mhp** (**M** = Ca, Ni, Zn) and **Mdchp** (**M** = Ca, Zn) complexes.

	Cahp	**Cadchp**	**Nihp**	**Znhp**	**Zndchp**	**H_2hp**	**H_2dchp**
Pyrrole	3.3	2.1	4.6	2.9	2.6	1.6	1.0
Benzene (isoindolic)	–7.6	–7.8	–7.7	–7.4	–7.6	–7.4	–7.8
Pyridine/benzene	–4.1	–8.0	–1.7	–2.2	–6.0	–4.4	–7.4
Internal cross*	3.0	–2.6	–1.0	6.2	0.4	3.7	0.0

* Since the metal atoms are located at the centers of complexes, NICS criteria of internal cross were measured at the geometric mean of two adjacent C_α–N and N_p–C_2 (for **hp** complexes) or C_α–N and C_1–C_2 (for **dchp** complexes) bonds.

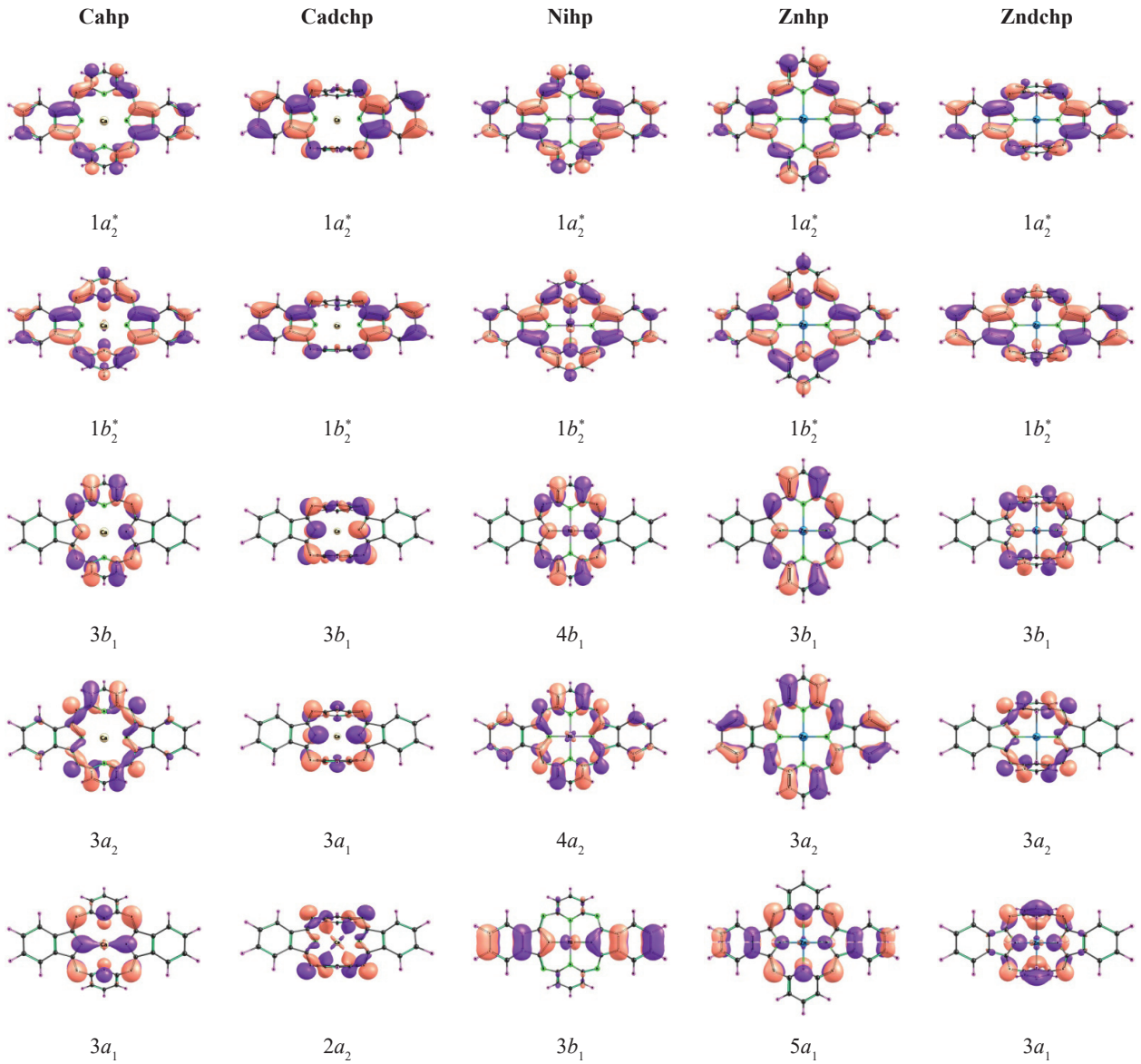

Figure 7. Influence of the metal (Ca, Ni, Zn) and ligand (**hp/dchp**) on the molecular orbitals of **Mhp** and **Mdchp** complexes.

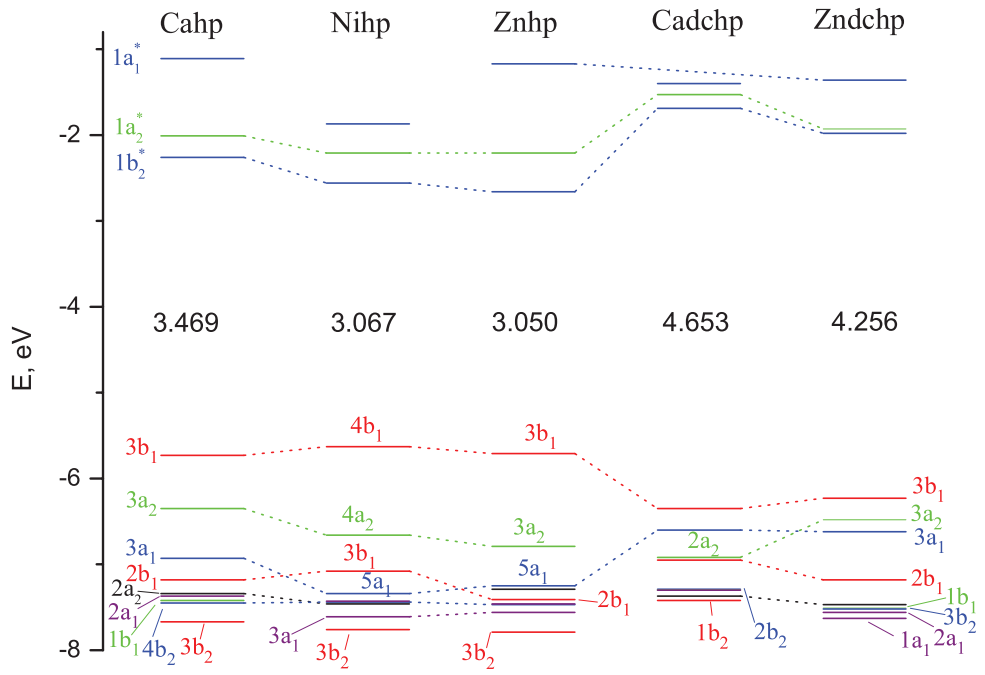

Figure 8. Molecular orbital (MO) level diagram for **Mhp** (**M** = Ca, Ni, Zn) and **Mdchp** (**M** = Ca, Zn) complexes. The values of highest occupied molecular orbital-lowest unoccupied molecular orbital (HOMO-LUMO) gaps are given in eV.

of the types σ(C–H) → 4*s*(Zn), σ(C–H) → 4*s*(Zn). This type of interaction was found in **dchp** complexes with Ag(I), Mn(II), Fe(II) and Co(II).[44,45]

The concept of aromaticity is widely used in the chemistry of the porphyrazines and their analogues.[46–49] The nucleus-independent chemical shift (NICS(0)) values calculated at the centers of cyclic fragments demonstrate the conservation of the aromatic properties of benzene fragments belonging to isoindole moieties of **hp** and **dchp** complexes and the absence of aromaticity in pyrrole fragments. It should be noted that the oppositely placed benzene moieties in **dchp** complexes with Ca and Zn are less aromatic as compared to benzene. In the very recent study[50] insertion of a metal atom into macrocyclic core was found to increase aromatic properties as compared to a free-base macrocycle. However the complexes of **H_2hp** and **H_2dchp** with Ca(II), Ni(II) and Zn(II) do not exhibit an unambiguous trend (Table 4).

Molecular Orbitals

The symmetry of the frontier molecular orbitals is similar in the all considered **Mhp** and **Mdchp** complexes: the highest occupied molecular orbital (HOMO) is b_1 orbital and the lowest unoccupied molecular orbital (LUMO) possesses b_2^* symmetry (Figure 7). Among the other near-frontier MOs, none can be assigned to Gouterman type[51,52] orbitals localized on the nitrogen atoms of the macrocycles. HOMO-LUMO gaps in **Mdchp** are significantly larger (~1.2 eV) compared to **Mhp** complexes (Figure 8).

Electronic Absorption Spectra

The influence of the natures of a metal atom and a ligand on the electronic absorption spectrum is expressed by Figure 9. The calculated oscillator strengths (f) for the lowest excited states along with their composition (in terms of one-electron transitions) are given in Table 5.

The HOMO–LUMO gap of the complexes studied is significantly higher than that of other complexes of macroheterocycles with metals.[20,53–55] This explains the fact that the Q absorption band is absent in the electronic spectra of these compounds. The strongest absorption maxima in the spectra of **Mhp** complexes in the near-UV region (300–420 nm) can be assigned to transitions between HOMO and LUMO+1 ($b_1 \rightarrow a_2^*$). Since these electronic transitions are not transitions between HOMO and LUMO, the correlation between the value of HOMO–LUMO gap and wavelengths of absorption bands is not observed.

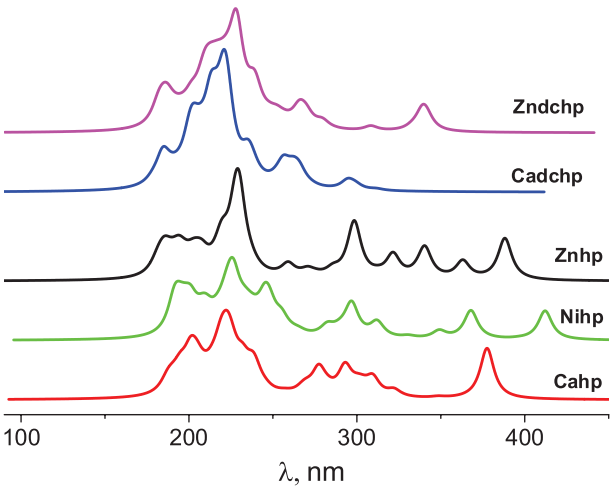

Figure 9. Calculated TDDFT electronic absorption spectra for **Mhp** and **Mdchp** complexes.

Table 5. Calculated composition of the lowest excited states and corresponding oscillator strengths for **Mhp** (M = Ca, Ni, Zn) and **Mdchp** (M = Ca, Zn) complexes.

State	Composition, %	λ, nm	f	Experimental λ, nm
	Cahp			
1^1B_2	$5b_1 \rightarrow 1a_2^*$ (95)	378	0.33	
4^1B_1	$3b_2 \rightarrow 1a_2^*$ (11) $1a_2 \rightarrow 1b_2^*$ (75)	293	0.30	
14^1B_1	$2b_2 \rightarrow 1a_2^*$ (8) $1a_2 \rightarrow 1b_2^*$ (7) $1b_1 \rightarrow 1a_1^*$ (45) $1a_1 \rightarrow 1b_1^*$ (7) $2b_1 \rightarrow 1a_1^*$ (8) $2b_1 \rightarrow 2a_1^*$ (6) $3a_1 \rightarrow 1b_1^*$ (24)	223	0.27	
	Nihp			
2^1B_2	$4b_1 \rightarrow 1a_2^*$ (95)	412	0.30	~ 455[55] DMSO
3^1B_1	$3a_2 \rightarrow 1b_2^*$ (4) $4a_2 \rightarrow 1b_2^*$ (92)	368	0.30	~ 420[55] DMSO
5^1B_2	$4a_1 \rightarrow 1b_2^*$ (5) $5a_1 \rightarrow 1b_2^*$ (84)	297	0.33	
	Znhp			
1^1B_2	$5a_1 \rightarrow 1b_2^*$ (5) $3b_1 \rightarrow 1a_2^*$ (94)	388	0.44	~ 396[55] DMSO
4^1B_2	$3a_1 \rightarrow 1b_2^*$ (18) $5a_1 \rightarrow 1b_2^*$ (72) $3b_1 \rightarrow 1a_2^*$ (5)	298	0.59	
9^1B_1	$2b_1 \rightarrow 1a_1^*$ (19) $5a_1 \rightarrow 1b_1^*$ (60) $3a_2 \rightarrow 2b_2^*$ (6)	230	0.71	
	Cadchp			
14^1B_1	$1a_1 \rightarrow 1b_1^*$ (6) $1a_2 \rightarrow 2b_2^*$ (5) $1b_1 \rightarrow 2a_1^*$ (5) $2a_1 \rightarrow 1b_1^*$ (54) $2b_1 \rightarrow 3a_1^*$ (10) $2a_2 \rightarrow 2b_2^*$ (6)	221	0.79	
17^1B_1	$1a_2 \rightarrow 2b_2^*$ (59) $1b_2 \rightarrow 2a_2^*$ (18) $2b_1 \rightarrow 3a_1^*$ (8)	213	0.53	
20^1B_1	$1b_2 \rightarrow 2a_2^*$ (72) $1b_1 \rightarrow 2a_1^*$ (17)	203	0.20	
	Zndchp			
1^1B_1	$3a_2 \rightarrow 1b_2^*$ (94)	341	0.11	335[56]
4^1B_1	$2b_2 \rightarrow 1a_2^*$ (10) $3b_2 \rightarrow 1a_2^*$ (9) $2a_2 \rightarrow 1b_2^*$ (42) $3b_1 \rightarrow 2a_1^*$ (13) $3b_1 \rightarrow 3a_1^*$ (11)	270	0.11	271[56]
15^1B_1	$1b_2 \rightarrow 1a_2^*$ (6) $2a_1 \rightarrow 1b_1^*$ (8) $3a_1 \rightarrow 2b_1^*$ (42) $3b_1 \rightarrow 3a_1^*$ (29)	217	0.21	
18^1B_1	$1a_2 \rightarrow 1b_2^*$ (11) $1a_1 \rightarrow 1b_1^*$ (25) $1b_1 \rightarrow 2a_1^*$ (41) $2b_1 \rightarrow 2a_1^*$ (5)	210	0.23	

Conclusions

The electronic structures of **Nihp** and **Nidchp** have been studied by CASSCF method followed by accounting for dynamic electron correlation by multiconfigurational quasidegenerate second-order perturbation theory (MCQDPT2). The wave functions of the ground state of **Nidchp** were found to possess a complex composition, therefore **Nidchp** could not be treated using single-reference DFT methods. Geometry and electronic structures of **Mhp** and **Mdchp** (M = Ca, Ni, Zn) complexes were described for the first time based on DFT/PBE0/pcseg-2 calculations except for **Nidchp**. The equilibrium structures of the studied complexes were determined to possess the saddle distorted structures of C_{2v} symmetry point group. The results of the NBO analysis of the electron density distribution indicate ionic character of Ca–N bonding in **Cahp** and **Cadchp**, while metal-ligand interactions in the case of Zn(II) and especially Ni(II) complexes possess pronounced covalent contribution. Larger stabilization of Nihp as compared to **Znhp** can be explained by additional LP(Np) → $3d_{x^2-y^2}$(Ni) and LP(Ni) → $3d_{x^2-y^2}$(Ni) interactions being absent in **Znhp**. The evidence of agostic interactions of the types σ(C–H) → 4*s*(Zn), σ(C–H) → 4*s*(Zn) in **Zndchp** predicted by E.S. Bonner *et al*.[30] was also found within the NBO method.

Acknowledgments. This work is supported by grant of the President of the Russian Federation (project MK-586.2020.3). Preliminary calculations is supported by the Russian Science Foundation under grant No. 17-73-10198.

References

1. Fernández-Lázaro F., Torres T., Hauschel B., Hanack M. *Chem. Rev.* **1998**, *98*, 563–575.
2. De La Torre G., Vázquez P., Agulló-López F., Torres T. *J. Mater. Chem.* **1998**, *8,* 1671–1683.
3. Islyaikin M.K., Danilova E.A. *Russ. Chem. Bull.* **2007**, *56,* 689–706.
4. Ziegler C.J. In: *Handbook of Porphyrin Science, Vol. 17* (Kadish K.M., Smith K.M., Guilard R., Eds.) **2011**, p. 113–238.
5. Wu Y., Gai L., Xiao X., Lu H., Li Z., Mack J., Harris J., Nyokong T., Shen Z. *Chem. - An Asian J.* **2016**, *11*, 2113–2116.
6. Islyaikin M.K., Danilova E.A., Romanenko Y.V., Khelevina O.G., Lomova T.N. Synthesis, Structure Peculiarities And Biological Properties of Macroheterocyclic Compounds. In: *Chemical Processes with Participation of Biological and Related Compounds* **2008**, p. 219–270.
7. Dini D., Calvete M.J.F., Hanack M., Amendola V., Meneghetti M. *Chem. Commun.* **2006**, 2394–2396.
8. Britton J., Antunes E., Nyokong T. *J. Mol. Struct.* **2013**, *1047*, 143–148.
9. Huber S.M., Seyfried M.S., Linden A., Luedtke N.W. *Inorg. Chem.* **2012**, *51*, 7032–7038.
10. Muranaka A., Ohira S., Toriumi N., Hirayama M., Kyotani F., Mori Y., Hashizume D., Uchiyama M. *J. Phys. Chem. A* **2014**, *118*, 4415–4424.
11. Huber S.M., Mata G., Linden A., Luedtke N.W. *Chem. Commun.* **2013**, *49*, 4280–4282.
12. Liu W., Pan H., Wang Z., Wang K., Qi D., Jiang J. *Chem. Commun.* **2017**, *53*, 3765–3768.

13. Persico V., Carotenuto M., Peluso A. *J. Phys. Chem. A* **2004**, *108*, 3926–3931.
14. Zakharov A.V., Stryapan M.G., Islyaikin M.K. *J. Mol. Struct. THEOCHEM* **2009**, *906*, 56–62.
15. Dini D., Calvete M.J.F., Hanack M., Amendola V., Meneghetti M. *J. Am. Chem. Soc.* **2008**, *130*, 12290–12298.
16. Costa R., Engle J.T., Ziegler C.J. *J. Porphyrins Phthalocyanines* **2012**, *16*, 175–182.
17. Alekseeva S.V., Kuznetsova A.S., Koifman O.I., Islyaikin M.K. *Macroheterocycles* **2017**, *10*, 543–547.
18. Costa R., Schick A.J., Paul N.B., Durfee W.S., Ziegler C.J. *New J. Chem.* **2011**, *35*, 794–799.
19. Toriumi N., Muranaka A., Hirano K., Yoshida K., Hashizume D., Uchiyama M. *Angew. Chemie - Int. Ed.* **2014**, *53,* 7814–7818.
20. Otlyotov A.A., Ryzhov I.V., Kuzmin I.A., Zhabanov Y.A., Mikhailov M.S., Stuzhin P.A. *Int. J. Mol. Sci.* **2020**, *21*, 2923.
21. Zhabanov Y.A., Sliznev V.V., Ryzhov I.V., Stuzhin P.A. *J. Porphyrins Phthalocyanines* **2020**, *24*, 1164–1154.
22. Elvidge J.A., Linstead R.P. *J. Chem. Soc.* **1952**, 5008–5012.
23. Speakman J. *Acta Crystallogr.* **1953**, *6*, 784–791.
24. Peng S.-M., Wang Y., Chen C.-K., Lee J.-Y., Liaw D.-S. *J. Chinese Chem. Soc.* **1986**, *33*, 23–33.
25. Agostinelli E., Attanasio D., Collamati I., Fares V. *Inorg. Chem.* **1984**, *23*, 1162–1165.
26. Sripothongnak S., Barone N., Ziegler C.J. *Chem. Commun.* **2009**, 4584–4586.
27. Geiger D.K., Schmidt R.G. *Inorg. Chim. Acta* **1992**, *197,* 203–207.
28. Kieber-Emmons M.T., Riordan C.G. In: *Accounts of Chemical Research*, Vol. *40*, American Chemical Society, **2007**, p. 618–625.
29. Ruf M., Durfee W.S., Pierpont CG. *Chem. Commun.* **2004**, 1022–1023.
30. Bonner E.S., Engle J.T., Sripothongak S., Ziegler C.J. *Dalton Trans.* **2010**, *39*, 1932–1934.
31. Otlyotov A.A., Zhabanov Y.A., Pogonin A.E., Kuznetsova A.S., Islyaikin M.K., Girichev G.V. *J. Mol. Struct.* **2019**, *1184*, 576–582.
32. Kuznetsova A.S., Pechnikova N.L., Zhabanov Y.A., Khochenkov A.E., Koifman O.I., Aleksandriiskii V.V., Islyaikin M.K. *J. Porphyrins Phthalocyanines* **2019**, *23*, 296–302.
33. Jensen F. *J. Chem. Theory Comput.* **2014**, *10*, 1074–1085.
34. Pritchard B.P., Altarawy D., Didier B., Gibson T.D., Windus T.L. *J. Chem. Inf. Model.* **2019**, *59*, 4814–4820.
35. Schuchardt K.L., Didier B.T., Elsethagen T., Sun L., Gurumoorthi V., Chase J., Li J., Windus T.L. *J. Chem. Inf. Model.* **2007**, *47*, 1045–1052.
36. Granovsky AA. Firefly version 8, www. *http://classic.chem.msu.su/gran/firefly/index.html*.
37. Schmidt M.W., Baldridge K.K., Boatz J.A., Elbert S.T., Gordon M.S., Jensen J.H., Koseki S., Matsunaga N., Nguyen K.A., Su S., Windus T.L., Dupuis M., Montgomery J.A. *J. Comput. Chem.* **1993**, *14*, 1347–1363.
38. Zhurko G.A. Chemcraft – Graphical Program for Visualization of Quantum Chemistry Computations. *https://chemcraftprog.com*.
39. Sliznev V.V., Vogt N., Vogt J. *J. Mol. Struct.* **2006**, *780–781*, 247–259.
40. Glendening E.D., Badenhoop J.K., Reed A.E., Carpenter J.E., Bohmann J.A., Morales C.M., Weinhold F. *NBO7 Website: http://nbo7.chem.wisc.edu/*
41. Harvey J.D., Ziegler C.J. *Coord. Chem. Rev.* **2003**, *247*, 1–19.
42. Chmielewski P.J., Latos-Grazyński L. *Coord. Chem. Rev.* **2005**, *249*, 2510–2533.
43. Harvey J.D., Ziegler C.J. *J. Inorg. Biochem.* **2006**, *100*, 869–880.
44. Durfee W.S., Ziegler C.J. *J. Porphyrins Phthalocyanines* **2009**, *13*, 304–311.
45. Çetin A., Durfee W.S., Ziegler C.J. *Inorg. Chem.* **2007**, *46*, 6239–6241.
46. Cyrañski M.K., Krygowski T.M., Wisiorowski M., Van Eikema Hommes N.J.R., Von Ragué Schleyer P. *Angew. Chemie - Int. Ed.* **1998**, *37*, 177–180.
47. Feixas F., Matito E., Poater J., Solà M. *Chem. Soc. Rev.* **2015**, *44*, 6434–6451.
48. Otlyotov A.A., Merlyan A.P., Veretennikov V.V., Pogonin A.E., Ivanov E.N., Filippova Y.E., Zhabanov Y.A., Islyaikin M.K. *Macroheterocycles* **2018**, *11*, 67–72.
49. Casademont-Reig I., Woller T., Contreras-García J., Alonso M., Torrent-Sucarrat M., Matito E. *Phys. Chem. Chem. Phys.* **2018**, *20*, 2787–2796.
50. Bacilla A.C.C., Okada Y., Yoshimoto S., Islyaikin M.K., Koifman O.I., Kobayashi N. *Bull. Chem. Soc. Jpn.* **2021**, *94*(1), 34–43.
51. Gouterman M., Wagnière G.H., Snyder L.C. *J. Mol. Spectrosc.* **1963**, *11*, 108–127.
52. Gouterman M. *J. Mol. Spectrosc.* **1961**, *6*, 138–163.
53. Lebedeva (Yablokova) I.A., Ivanova S.S., Novakova V., Zhabanov Y.A., Stuzhin P.A. *J. Fluor. Chem.* **2018**, *214*, 86–93.
54. Zhabanov Y.A., Tverdova N.V., Giricheva N.I., Girichev G.V., Stuzhin P.A. *J. Porphyrins Phthalocyanines* **2017**, *21*, 439–452.
55. Sliznev V.V. *Macroheterocycles* **2013**, *6*, 111–122.
56. Sakata K., Gondo K., Hayashi Y., Hashimoto M. *Synth. React. Inorg. Met. Chem.* **1991**, *21*, 17–31.
57. Berezina G.R., Vorob'ev Y.G., Smirnov R.P. *Koord. Khim.* **1996**, *22*, 60–62.

Received 13.11.2020
Accepted 18.01.2021